Scientia Iranica A (2019) 26(4), 2229–2240

Sharif University of Technology
Scientia Iranica
Transactions A: Civil Engineering
http://scientiairanica.sharif.edu

Invited Paper

Numerical modeling of particle motion and deposition in turbulent wavy channel flows

H. Hayati[a,1], A. Soltani Goharrizi[a], M. Salmanzadeh[b], and G. Ahmadi[c,*]

a. *Department of Chemical Engineering, Shahid Bahonar University of Kerman, Kerman, Iran.*
b. *Department of Mechanical Engineering, Shahid Bahonar University of Kerman, Kerman, Iran.*
c. *Department of Mechanical and Aeronautical Engineering, Clarkson University, Potsdam, NY, USA.*

Received 2 March 2019; accepted 4 May 2019

KEYWORDS
Particle deposition;
Wavy channel;
Turbulent flow;
v2f turbulence model;
Aerosols.

Abstract. This work investigates the turbulent flow and particles deposition in wavy duct flows. The v2f turbulence model was used for simulating the turbulent flow through the wavy channel. The instantaneous turbulence fluctuating velocities were simulated using the Kraichnan Gaussian random field model. For tracking particles in the fluid flow, the particle equation of motion was solved numerically. The drag, Saffman lift, Brownian, and gravity forces acting on a suspended particle were included in the particle equation of motion. The effects of duct wave amplitude and wavelength on deposition of particles of different sizes were studied. A range of waves with different amplitudes and wavelengths was simulated. The particle tracking approach was validated for turbulent flow in a flat horizontal channel, where good agreement with previous studies was found. The presented results showed that the duct wavy walls significantly increased the particle deposition rate.

1. Introduction

In the last three decades, understanding particle dispersion and deposition has attracted considerable attention due to its numerous industrial, environmental, and biological applications. Many researchers have worked on computational modeling of dispersion and deposition of particles in the past. Wood [1] evaluated turbulent deposition in duct flows with smooth and rough walls. Fan and Ahmadi [2] and Li and Ahmadi [3] investigated particle deposition in vertical ducts with smooth and rough walls and concluded that the deposition rate increased as the roughness height increased. Tian and Ahmadi [4] compared different models for simulating particle deposition in turbulent duct flows and pointed out the issues with some of the models used in commercial codes. Zhang and Chen [5] simulated the flow field using the v2f turbulence model and reported particle movements using a modified Lagrangian approach. Gao and Li [6] studied particle deposition in vertical square ventilation duct flows and reported that the gravity would contribute to the effect of the Saffman lift force. Sun et al. [7] studied particle flows in a 90° bend using the Lagrangian-tracking model and included the particle-wall collision effects; they made reasonable predictions of particle distribution and deposition in the bend. Gao et al. [8] used the RSM, RNG $k-\varepsilon$, and SST $k-\omega$ models as well as the Lagrangian particle tracking method for evaluating particle deposition. Majlesara et al. [9]

1. *Present address: School of Chemical Engineering, Oklahoma State University, Stillwater, Oklahoma, US. 74075.*
*. *Corresponding author. Tel.: +1-315-268-2322*
E-mail addresses: Hamideh.hayati@okstate.edu (H. Hayati); a.soltani@uk.ac.ir (A. Soltani Goharrizi); msalmanz@uk.ac (M. Salmanzadeh); gahmadi@clarkson.edu (G. Ahmadi)

doi: 10.24200/sci.2019.21405

analyzed particle deposition in an inclined turbulent channel flow. They evaluated the instantaneous velocity field using the Kraichnan Gaussian Random field model. Generally, investigations into turbulent flows in wavy channels have attracted considerable attention.

Cherukat et al. [10], Yoon et al. [11] and Errico and Stalio [12] simulated the turbulent flows in channels with wavy walls using the Direct Numerical Simulation. They reported the details of dynamics of fluid flows for different wave amplitudes. Lu and Lu [13] numerically compared the particle deposition rates in turbulent duct flows with smooth wall and those with ribbed wall. They found that the deposition rate of particles was enhanced by surface ribs, especially in turbulent eddy impact regimes. Lu and Lu [14] investigated the effects of surface rib shapes on particle deposition in turbulent dust flows utilizing the Reynolds Stress Transport Model (RSTM). They concluded that the square-shape ribs led to the maximum enhancement of particle deposition rate compared to the other rib shapes.

Ni et al. [15] studied particle deposition in liquid flows in a horizontal channel. They concluded that both the wall roughness and thermophoresis had a significant impact on deposition rate of fine particles. Wang et al. [16] studied particle deposition in a ventilation duct with a convex wall cavity. They found that the deposition rate considerably increased in wall cavities. Dritselis [17] studied particle deposition in a turbulent channel flow with rough walls. It was shown that particles accumulation in the near-wall region was significantly affected by the roughness elements. Dritselis [18] reported on the enhancement of deposition rate of particles in turbulent channel flow with a ribbed wall. The increase in particle deposition was related to the direct inertial impaction and interception mechanisms. Li et al. [19] performed direct numerical simulation of polydispersed particle deposition in low-Reynolds-number turbulent flows. They indicated that for particles larger than 10 μm, the gravity was the main deposition mechanism for Re $<$ 6000. Ho et al. [20] studied particle deposition in wavy channels and concluded that windward surfaces were the main deposition regions. Gu et al. [21] used a stochastic model for simulating particle transport and deposition in wall-bounded turbulent flows. Lu et al. [22] numerically investigated the deposition of monodispersed particles in turbulent duct flow and included the thermophoretic force. They found that for particles smaller than 10 μm, the thermophoretic force had significant effects, while for particles larger than 10 μm, it was negligible. Wang et al. [23] performed a large eddy simulation of deposition and resuspension of 5 to 500 μm particles in turbulent duct flows. For 5 μm particles, the deposition rates on all the walls (ceiling, vertical walls, and floor) were similar and increased with the flow Reynolds number.

In this study, simulations of micro-particle deposition in turbulent flows in wavy ducts were presented. The fluid flow was simulated using the ANSYS-FLUENT software by the v2f turbulence model. The fluctuation velocity field was generated by the Kraichnan Gaussian Random field model. Lagrangian particle tracking approach was used and the particle deposition velocity as a function of particle relaxation time was evaluated. The simulation results were compared with the available experimental data and reasonable agreement was found.

2. Turbulent flow field

The mean fluid flow was evaluated by solving the coupled continuity and Reynolds Averaged Navier-Stokes (RANS) equations as well as the energy equation. Details of the governing equations may be found in Fluent manual; they are not reported here for the sack of brevity. It is known that the turbulent flows in the near-wall region are strongly anisotropic. Therefore, it is important to use a turbulence model that accounts for the anisotropy effects, especially near the wall. The simplest model that accounts for the turbulence anisotropy is the v2f model introduced by Durbin [24], which solves three transport equations for turbulence kinetic energy, k, turbulence dissipation, ε, and variance of fluctuation velocity normal to the wall, $\overline{v'^2}$, and an elliptic equation for the relaxation function, f. Following Majlesara et al. [9], the turbulence kinetic energy, k, and the wall-normal stress, $\overline{v'^2}$, are used for simulating the instantaneous turbulent velocity field.

Small particles movements through turbulent flows are influenced by the instantaneous fluid velocity. In this study, for generating the instantaneous velocity fluctuations, the continuous Gaussian random field model of Kraichnan [25] is used. The non-dimensional form of Gaussian random field is given as:

$$\overrightarrow{u}^{I*}\left(\overrightarrow{x^*},t^*\right)=\sqrt{\frac{2}{N}}\left\{\sum_{n=1}^{N}\overrightarrow{u_1}\left(\overrightarrow{k_n}\right)\cos\left(\overrightarrow{k_n}\overrightarrow{x^*}+\omega_n t^*\right)+\sum_{n=1}^{N}\overrightarrow{u_2}\left(\overrightarrow{k_n}\right)\sin\left(\overrightarrow{k_n}\overrightarrow{x^*}+\omega_n t^*\right)\right\}, \quad (1)$$

where:

$$\overrightarrow{u_1}\left(\overrightarrow{k_n}\right)=\overrightarrow{\zeta_n}\times\overrightarrow{k_n},\qquad \overrightarrow{u_2}\left(\overrightarrow{k_n}\right)=\overrightarrow{\xi_n}\times\overrightarrow{k_n}, \quad (2)$$

and incompressibility is ascertained by:

$$\overrightarrow{k_n}\cdot\overrightarrow{u_1}\left(\overrightarrow{k_n}\right)=\overrightarrow{k_n}\cdot\overrightarrow{u_2}\left(\overrightarrow{k_n}\right)=0, \quad (3)$$

where $\overrightarrow{\zeta_n}$, $\overrightarrow{\varepsilon_n}$, and the frequencies, ω_n, are selected from a population of zero-mean, unit-variance Gaussian random numbers. Here, $\overrightarrow{k_n}$ is a random vector whose components are also zero-mean Gaussian random numbers with the variance of 0.25. In Eq. (1), the dimensionless parameters are defined as:

$$x^* = x/l_0, \qquad t^* = t/t_0, \qquad u_i^{I*} = u_i^v/u^*, \tag{4}$$

where u_i^v is the instantaneous velocity. Here, the length, time, and velocity scales of turbulence are respectively l_0, t_0, and u^*. According to Davies [26], for a duct flow, $l_0 = 0.1h(2\mathrm{Re})^{-1/8}$, $t_0 = \frac{h}{2u_m}$, and shear velocity, $u^* = \sqrt{\frac{\tau_w}{\rho_f}}$, are used. Here, u_m is average velocity in the duct, h is the channel half-width, $\mathrm{Re} = \frac{u_m h}{v}$, and τ_w is the wall shear stress obtained from the simulations evaluated by the v2f turbulence model.

Majlesara et al. [9] suggested using:

$$e_1(\overrightarrow{x}) = \sqrt{2\left(k - \overline{v'^2}\right)}, \qquad e_2(\overrightarrow{x}) = \sqrt{\overline{v'^2}}. \tag{5}$$

Here, $e_1(\overrightarrow{x})$ and $e_2(\overrightarrow{x})$ are root mean-square turbulence fluctuations in the stream-wise and normal directions. Using the expression of Kraichnan [25] given by Eq. (1) and turbulence intensities given by Eq. (5), the velocity fluctuations in stream-wise and normal directions are generated. That is:

$$u_i' = u_i^{I*} e_i(x). \tag{6}$$

Then, instantaneous velocity is obtained as:

$$u_i = \overline{u}_i + u_i', \tag{7}$$

where u_i' is fluctuation velocity and $\overline{u}_i$ is mean flow velocity. The instantaneous velocity is used in the particle equation of motion and the corresponding particle trajectories are evaluated.

3. Lagrangian particle trajectory analysis

3.1. Particle equations of motion

The Lagrangian equation of motion of a particle suspended in a fluid is given as:

$$\frac{du_i^p}{dt} = \frac{1}{\tau}\frac{C_D \mathrm{Re}_p}{24}\left(u_i^f - u_i^p\right) + \frac{g_i(\rho_p - \rho_f)}{\rho_p} + n_i(t) + F_{Li}, \tag{8}$$

$$\frac{dx_i}{dt} = u_i^p, \tag{9}$$

where u_i^p and u_i^f are, respectively, the particle and the instantaneous fluid velocities. The left-hand side of Eq. (8) represents the particle acceleration, and the first term on the right-hand side is the drag force. Here, τ is the particle relaxation time and C_D is the drag coefficient. The drag coefficient, C_D, is given as:

$$C_D = \frac{24}{\mathrm{Re}_p} \qquad \text{for } \mathrm{Re}_p < 1, \tag{10}$$

$$C_D = \frac{24}{\mathrm{Re}_p}\left(1 + 0.15\mathrm{Re}_p^{0.687}\right) \qquad \text{for } 1 < \mathrm{Re}_p < 400, \tag{11}$$

where $\mathrm{Re}_p = \frac{d_p|u_i^f - u_i^p|}{\nu}$. Here, ν is the fluid kinematic viscosity.

The second term on the right-hand side of Eq. (8) is the gravity force (including buoyancy), where ρ_f and ρ_p are, respectively, the densities of air and particle. The last two terms on the right side of Eq. (8), namely $n_i(t)$ and F_{Li}, are, respectively, the Brownian and the shear induced lift forces per unit mass.

The particle relaxation time is defined as:

$$\tau = \frac{S d_p^2 C_c}{18\nu}, \tag{12}$$

where S is particle to fluid density ratio and C_c is the Stokes-Cunningham slip correction factor given as:

$$C_c = 1 + \frac{2\lambda}{d_p}\left(1.257 + 0.4e^{\frac{-1.1 d_p}{2\lambda}}\right). \tag{13}$$

Here, λ is the air mean free path.

As noted before, particles in a shear field experience a lift force perpendicular to the flow direction. The Saffman [27] shear lift force is given as:

$$F_{Li} = 1.615\rho_f \nu^{0.5} d_p^2 (u_i^f - u_i^p)\sqrt{\frac{du_i^f}{dx_i}}\,\mathrm{sign}\left(\frac{du_i^f}{dx_i}\right), \tag{14}$$

where the term $\frac{du_i^f}{dx_j}$ is the shear rate (note that only the near-wall lift with $i = 1$ and $j = 2$ is used).

The amplitude of Brownian force modeled as white noise process is given as [3]:

$$n_i(t) = G_i\left(\frac{\pi S_0}{dt}\right)^{1/2}, \tag{15}$$

where the spectral intensity of the noise is given by:

$$S_0 = \frac{216\nu kT}{\pi^2 \rho d_p^5 s^2 C_c}. \tag{16}$$

In Eq. (15), G_i is picked at every time step from a population of zero-mean Gaussian random numbers with unit variance. In Eq. (16), $k = 1.38 \times 10^{-23}$ J/k is the Boltzmann constant, T is the absolute temperature, and d_p is the particle diameter.

3.2. Particle deposition

Particles transported by turbulent flows in channels are deposited on the walls due to turbulence and other forces. The rate of particles deposition depends on particle size and density and the intensity of turbulence. The dimensionless form of the deposition velocity is defined as:

$$u_d^+ = \frac{J}{C_0 u^*}. \tag{17}$$

Here, J is the flux to the wall, C_0 is the particle concentration, and u^* is the shear velocity. Note that + superscript indicates the wall units, implying that the quantity is non-dimensionalized using u^* and kinematic viscosity ν. In Lagrangian particle tracking approach, the non-dimensional deposition velocity may be evaluated by the use of the equation suggested by Li and Ahmadi [3]. That is:

$$u_d^+ = \frac{N_d/t_d^+}{N_o/y_0^+}. \tag{18}$$

Here, N_o particles are injected randomly within the distance of y_0^+ from the wall and N_d is the number of deposited particles in time duration, t_d^+. The time duration t_d^+ is selected when the slope N_d/t_d^+ reaches a constant.

4. Results and discussion

In order to study the effects of amplitude and wavelength of the sinusoidal waves on particle deposition, different 2-dimentional wavy wall channels were simulated. In order to reach fully developed condition for flat horizontal channel and quasi-fully developed condition for wavy horizontal channel, and to omit the entrance region effects, turbulent flows were simulated in channels that were 0.02 m in height and 1 m in length. However, particle tracking was performed in the last 40 cm of the channels, as illustrated in Figure 1.

4.1. Fluid flow

To test the accuracy of the computational model, turbulent flow in a 2-dimensional channel with flat walls was first simulated. The flat channel was 2 m long with a height of 0.02 m. Particle transport and deposition were studied in the last 0.4 m of the channel, where the flow was nearly fully developed. The flow mean velocity was 5 m/s with Re = 6850. No-slip boundary condition was applied to the lower and upper walls. For the case of a flat channel, the symmetry boundary condition was used in order to reduce the number of grids and simulation time.

A computational grid with 13,800 cells was used. The grid near the wall was finer than that in the core region. The distance of the first grid from the wall was 0.1 mm, corresponding to $y^+ = yu^*/\nu = 1$. The mean velocity and turbulence kinetic energy profiles that were used by Tian and Ahmadi [4] were applied in the present work as the inlet boundary condition for the duct flow.

Figure 2 compares the simulated velocity profile of flat channel with those of Philips et al. [28] and Majlesara et al. [9] as well as the standard near-wall linear and log profiles given as:

$$\begin{cases} u^+ = y^+ & \text{for } y^+ < 11.225 \\ u^+ = \frac{1}{k}\ln(Ey^+) & \text{for } y^+ > 11.225 \end{cases} \tag{19}$$

where $k = 0.42$ and $E = 9.81$. As it is observed in Figure 2, the prediction of the present model is in good agreement with the simulation of Philips et al. [28], but there are some small deviations from the standard wall function and the earlier study of Majlesara et al. [9]. This points to some limitations of the present v2f turbulence model.

Figure 3 compares the predicted non-dimensional Root Mean-Square (RMS) fluctuation velocities with the earlier simulations. Here, $U'^+ = \frac{\sqrt{<u'^2>}}{u^*}$ and $V'^+ = \frac{\sqrt{<v'^2>}}{u^*}$, where angular bracket stands for

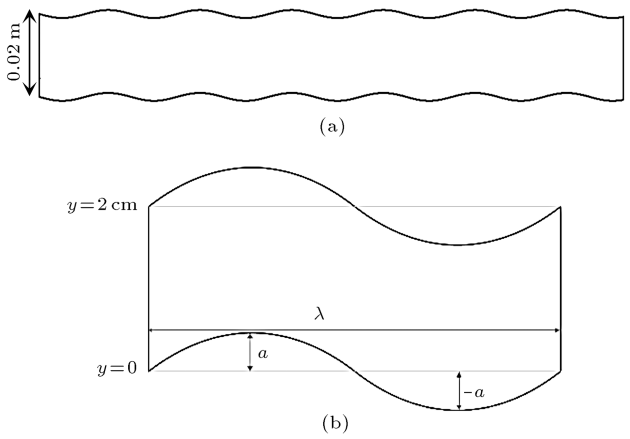

Figure 1. (a) Schematic of the segment of the wavy channel that is used for particle tracking (vertical scale is enlarged). (b) Schematic of one wave.

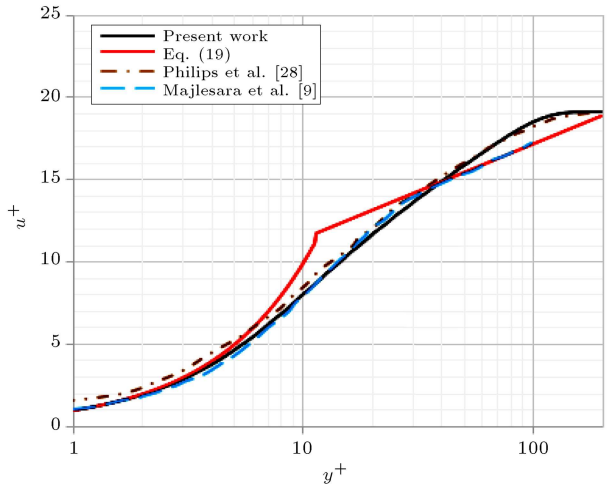

Figure 2. Comparison of the mean flow velocity obtained by the present v2f simulation with the standard wall function given by Eq. (19).

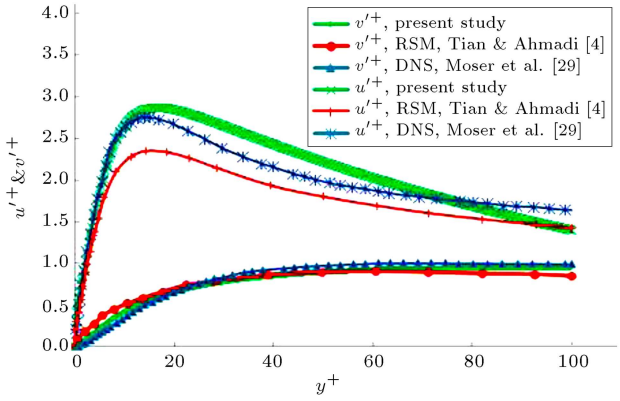

Figure 3. Non-dimensional RMS fluctuation velocities in stream-wise and wall normal directions for fully developed channel flow with flat walls.

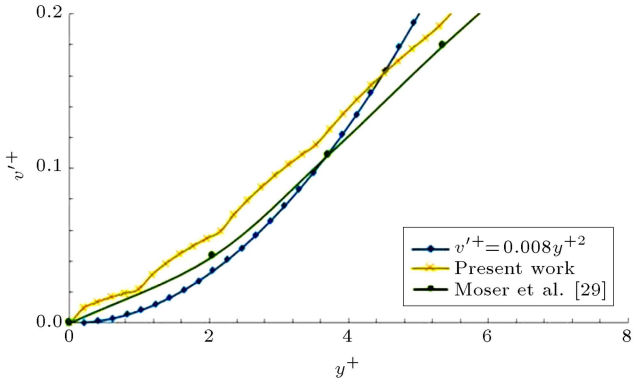

Figure 4. Comparison of the values of v'^+ predicted by the v2f turbulence model with the results of the DNS by Moser et al. [29] and $v'^+ = 0.008y^{+2}$ by Ounis et al. [30].

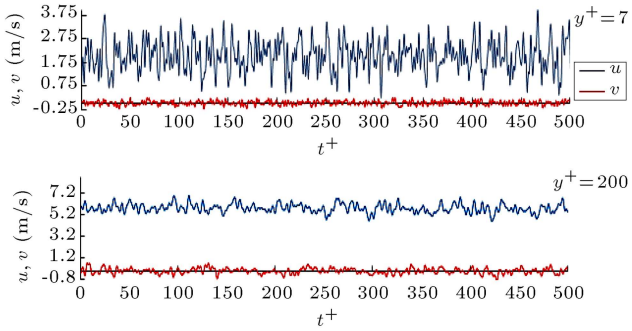

Figure 5. Time variations of the simulated instantaneous velocity versus non-dimensional time at different locations.

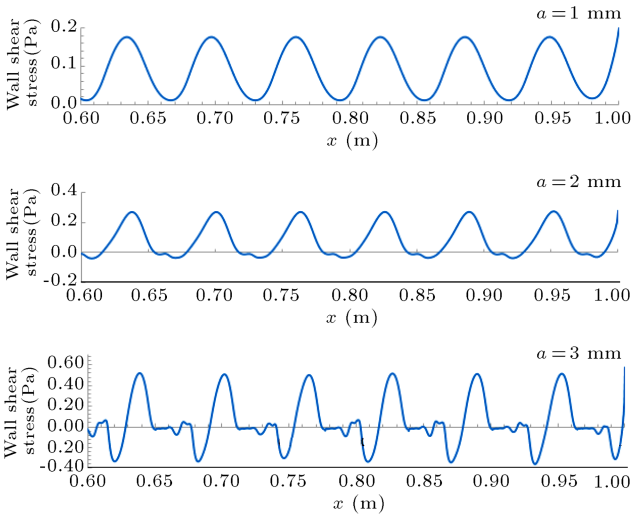

Figure 6. Variations of shear stress along the channel length; mean velocity = 5 m/s, $\lambda = 62.8$ mm.

expected value and u^* is the shear velocity. This figure shows that turbulence fluctuation intensity in the flow direction is much larger than that in the perpendicular direction, especially in the near-wall regions. It is also observed that there is a good agreement between the present simulation, the Direct Numerical Simulation (DNS) of Moser et al. [29], and the RSTM results of Tian and Ahmadi [4]. As it is expected, in the core region of the turbulent channel flow, fluctuation velocities tend to be isotropic, while in the near-wall region, they are highly anisotropic. The present v2f model seems to properly predict the sharp increase in the stream-wise fluctuation velocity from core region of the channel to the wall vicinity and then, its rapid decrease to zero on the wall.

Figure 4 compares the non-dimensional RMS fluctuation velocities in the normal direction near the wall obtained by the v2f turbulence model with those by DNS proposed by Moser et al. [29] and the equation $v'^+ = 0.008y^{+2}$ suggested by Ounis et al. [30] based on their DNS. It is seen that the prediction of the model is in general agreement with the DNS results.

To provide an insight into the time evolution of the fluctuation velocities, two sample-simulated instantaneous velocities at $y^+ = 7$ and $y^+ = 200$ are shown in Figure 5. It is seen that the Kraichnan model provides rather smoothly varying velocity fluctuations. As expected, the intensities of the velocity fluctuations in stream-wise and vertical directions at the channel center ($y^+ = 200$) are comparable, whereas in the near-wall region ($y^+ = 7$), the magnitude of v' is noticeably smaller than that of u'. It is also observed that the intensity of stream-wise velocity fluctuations in the near-wall region is much higher than that in the core region.

For the wavy wall case, the wall shear stresses for different wall wave amplitudes are evaluated and the results for the last 40 cm of the channel are shown in Figure 6. In this figure, a and λ are, respectively, the amplitude and the wavelength of the wavy wall. Unless stated otherwise, the wavelength is kept fixed at 0.0628 m in this study. It is seen that the wall shear stress roughly varies periodically. Also, a larger amplitude of the wavy wall leads to higher amplitude of the wall shear stress. In addition, for larger wall amplitudes, secondary fluctuations in the wall shear

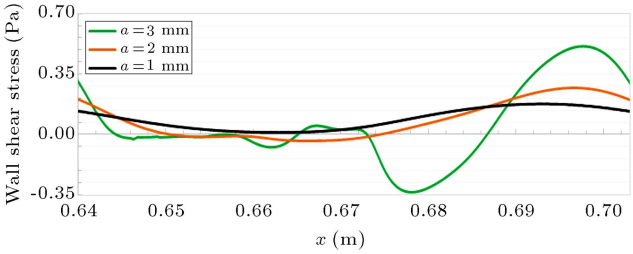

Figure 7. Comparison of variations of wall shear stresses for different amplitude waves versus x in one wavelength, $\lambda = 62.8$ mm.

stress appear that could generate negative wall shear stress in certain areas, perhaps due to the formation of recirculating flow regions.

Figure 7 compares the details of the trend of wall shear stress variation for one wavelength (0.644 m $<$ x $<$ 0.707 m) in channels with different wave amplitudes. It is observed that by increasing the wave amplitudes, variations of wall shear become more complex and regions with negative shear stresses appear. This is because as the amplitude increases, a strong adverse pressure gradient appears that leads to flow separation and formation of recirculating regions. In these regions, with reverse flows, the wall shear stress becomes negative. At the points of separation and/or reattachment, the velocity gradient and the wall shear stress become zero.

Figure 8 shows the non-dimensional mean stream-wise velocity profiles in turbulent wavy channels with $\frac{2a}{\lambda} = 0.0318$ ($a = 1$ mm, $\lambda = 6.28$ mm), $\frac{2a}{\lambda} = 0.0637$ ($a = 2$ mm, $\lambda = 62.8$ mm), and $\frac{2a}{\lambda} = 0.0955$ ($a = 3$ mm, $\lambda = 62.8$ mm) at three consecutive cross sections at crests of the top wall waves. The case of $\frac{2a}{\lambda} = 0.2$ ($a = 2$ mm, $\lambda = 20$ mm) is also added for comparison with the cases that the wavelength of the wall is much shorter. It is seen that the mean velocity is not symmetric and is fuller near the lower wall at the crest of the wave; also, it is generally lower in the trough of the wave on the upper wall. For larger values of $\frac{2a}{\lambda}$, the stream-wise velocity is negative near the upper wall due to the formation of recirculating flows in the troughs. Figure 8 also shows that the velocity profiles in the consecutive sections are nearly the same and the flow is in the quasi-fully developed condition in the stream-wise direction. Note that for the channel with $\frac{2a}{\lambda} = 0.2$ ($a = 2$ mm, $\lambda = 20$ mm), it is not necessary to lengthen the channel, because the quasi-fully developed condition is reached in the channel of 0.4 m length.

Figure 9 shows the velocity contour in four channels with different amplitudes and wavelengths. It

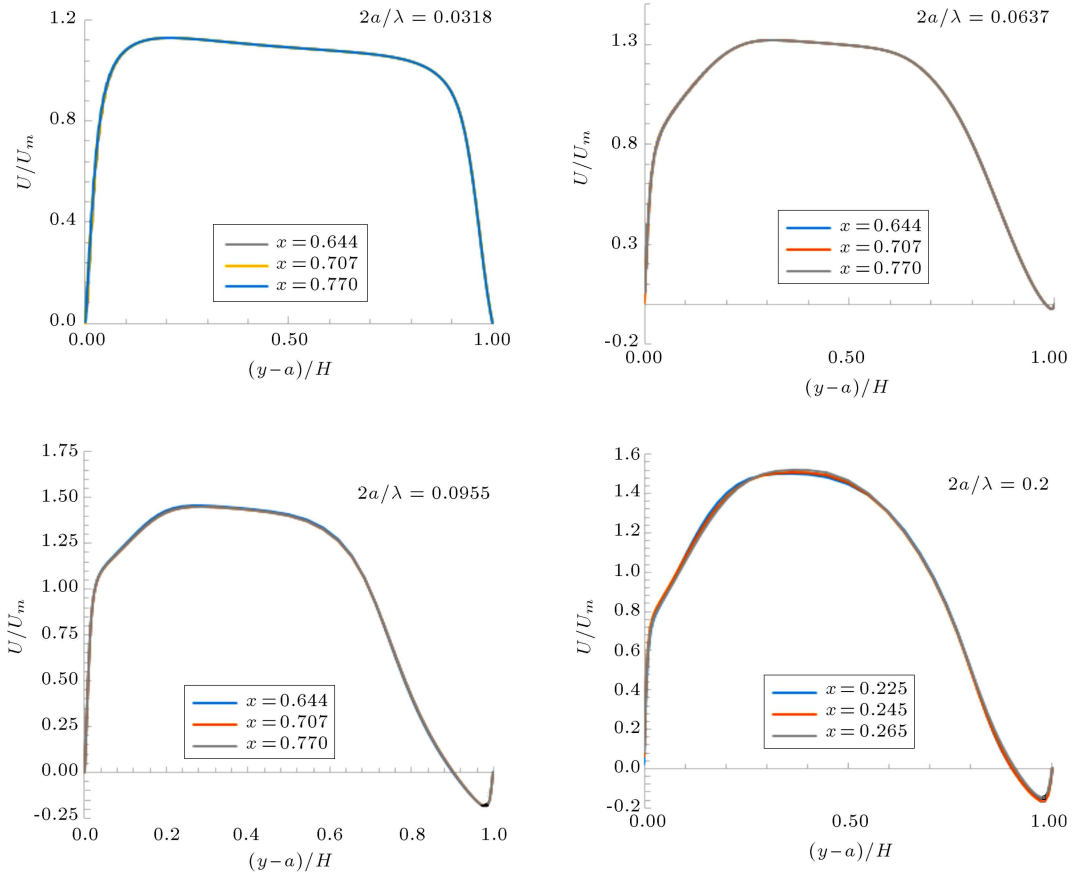

Figure 8. Dimensionless velocity profile versus dimensionless distance from wall.

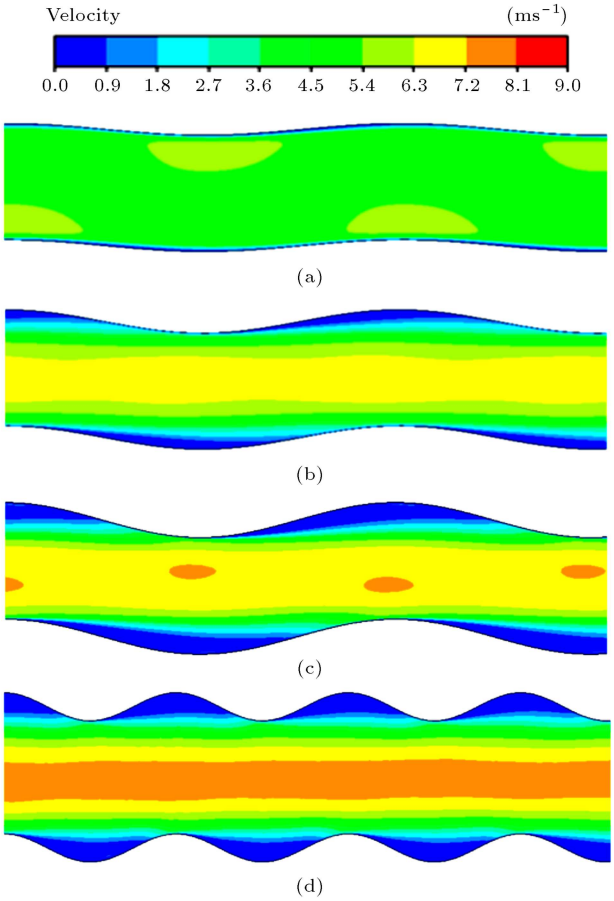

Figure 9. Velocity magnitude contours in wavy channels with different amplitudes and wavelengths: (a) $\frac{2a}{\lambda} = 0.0318$, (b) $\frac{2a}{\lambda} = 0.0637$, (c) $\frac{2a}{\lambda} = 0.0955$, and (d) $\frac{2a}{\lambda} = 0.2$.

is observed that for small values of $\frac{2a}{\lambda}$, the velocity contour, similar to that in the straight channel with high velocity in the core region, sharply approaches zero at the wall. For increasing values of $\frac{2a}{\lambda}$, low-velocity regions in the concave parts of the wall are formed, which could contain recirculating flow fields. These trends can be more clearly observed for $\frac{2a}{\lambda} = 0.0955$ and, particularly, $\frac{2a}{\lambda} = 0.2$.

Figures 10 and 11 show the RMS fluctuation velocity profiles versus the distance from wall at the trough and crest of the lower wall, respectively, in the wavy wall channels. It is seen that the RMS velocities reach their peak values near the wall and then, decrease toward the core. For low wave amplitudes such as $\frac{2a}{\lambda} = 0.0318$, the RMS velocity fluctuations are similar to those for flat channel shown in Figure 3. With increase in the wave amplitude and wavelength, the fluctuation velocities in both directions increase. The direct numerical simulation results of Cherukat et al. [10] for turbulent flow over the trough and crest sections are shown in Figures 10 and 11 for comparison with the present simulations for the case of $\frac{2a}{\lambda} = 0.1$ ($a = 1$ mm, $\lambda = 20$ mm). The experimental data of Hudson [31] are also shown by symbols. It is seen that the results of the present simulation are in general agreement with the experimental data and earlier DNS study of Cherukat et al. [10]. There are, however, some differences between the present v2f simulations and the earlier DNS and experimental studies, which are perhaps due to the differences in geometry. Figures 10 and 11 also show that by reducing $\frac{2a}{\lambda}$ (reducing the wave amplitude or increasing the wavelength), the peak of the RMS fluctuation velocities reduces and location of the peak moves further from the wall, especially at the trough of the walls. In addition, it is observed that both Urms/Um and Vrms/Um in the trough and crest sections of the wall have approximately the same maximum values. Both Urms and Vrms reach their peak values at the points closer to the wall at the crest than at the trough of the wall.

Close examination of the flow streamlines near the wall shows that the flow in the wavy channel with the small value of amplitude ratio of $\frac{2a}{\lambda} = 0.0318$ does not produce circulation regions. This is due to the small amplitude of the wave and absence of flow separation.

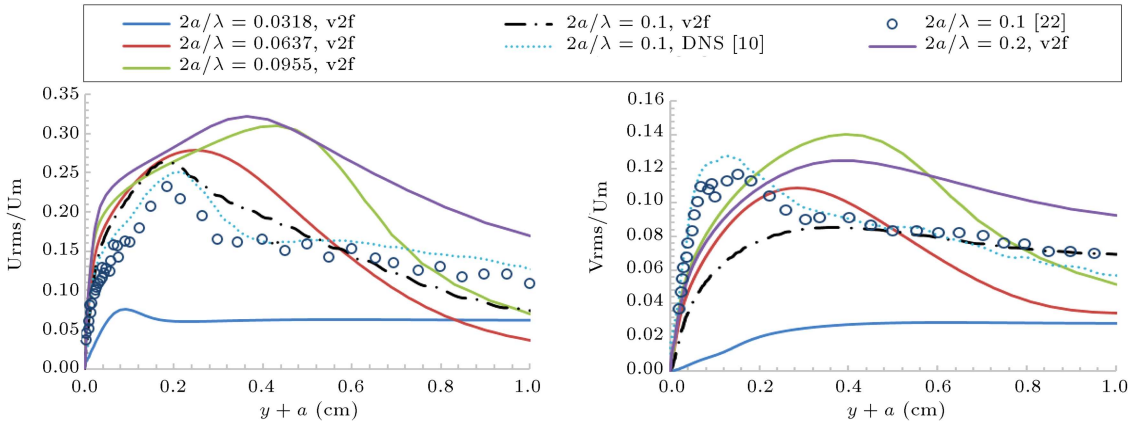

Figure 10. Non-dimensional fluctuation velocity intensities in stream-wise and wall normal directions at the trough of the lower wall for quasi-fully developed wavy horizontal channel flows.

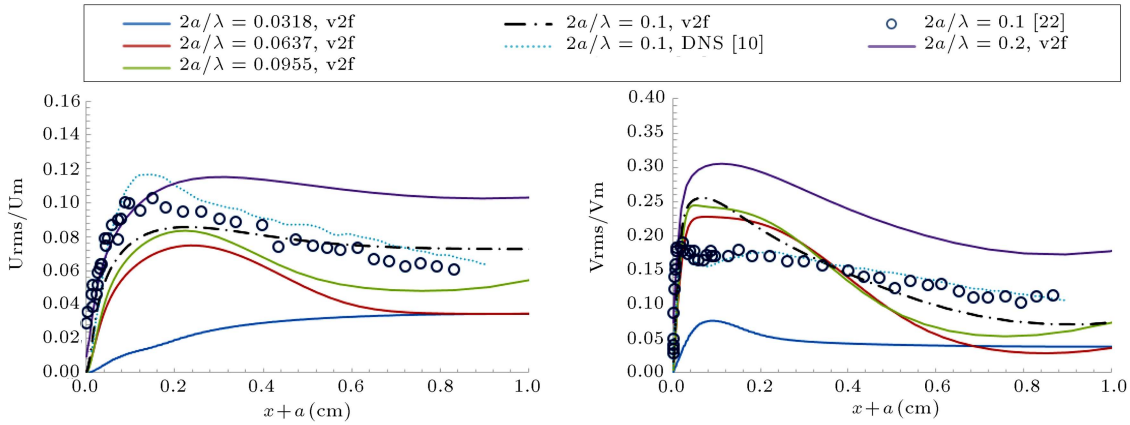

Figure 11. Non-dimensional fluctuation velocity intensities in stream-wise and wall normal directions at the crest of the lower wall for quasi-fully developed wavy horizontal channel flows.

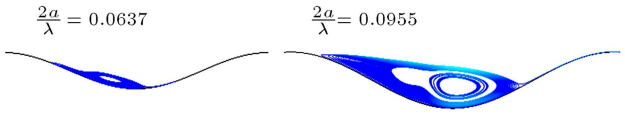

Figure 12. Recirculation region in the concave region of the wavy wall for large $\frac{2a}{\lambda}$.

However, the streamlines shown in Figure 12 indicate that when the amplitude increases to $\frac{2a}{\lambda} = 0.0637$ and 0.0955, a circulation region in the trough area is formed. Figures 6 and 7 show that in these cases, parts of the trough region experience negative wall shear stress due to the flow separation and formation of recirculating regions.

4.2. Particle trajectory analysis

A homemade MATLAB code for particle tracking in the wavy channel has been developed and used in the present study. The new code solves the particle equation of motion, including the drag, Brownian, gravity, and Saffman lift forces. To check the accuracy of the MATLAB code, the case of a flat horizontal channel is first simulated. The data for the turbulent flow field are exported from the ANSYS-FLUENT code and used in the particle trajectory analysis.

Five thousand particles were injected randomly across the channel within the distance of 0.0015 m (corresponding to $y^+ = 30$) from the bottom wall of the flat channel. The initial velocities of particles were same as those of the fluid at the points the particles were injected. The resulting particle trajectories were analyzed and their deposition velocities were evaluated. The results are plotted in Figure 13 and compared with earlier results and empirical model predictions. In the present simulations, the flow shear velocity in the flat horizontal channel is $u^* = 0.3$ m/s. This figure shows that the deposition velocity follows a V-shape curve, with high deposition rate for very small particles due to Brownian motion, decreasing with size

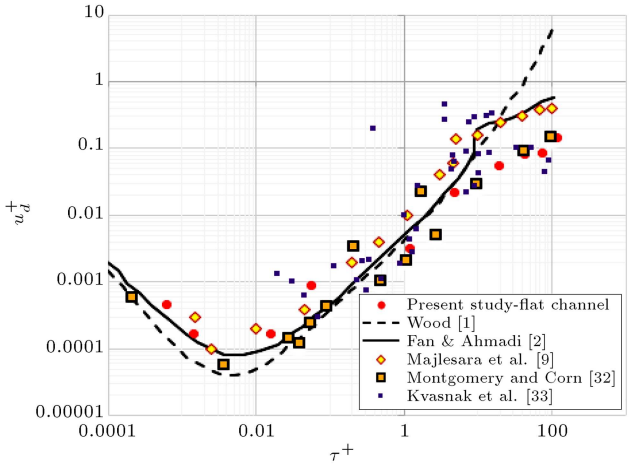

Figure 13. Variation of non-dimensional deposition velocity versus non-dimensional relaxation time in a horizontal flat channel.

to a minimum of about 6×10^{-5} for $\tau^+ \cong 0.006$. Then, it sharply increases with increase in particle relaxation time due to the turbulent inertia impaction and gravitational sedimentation. Figure 13 also shows that the predicted non-dimensional particle deposition velocity agrees with the empirical equations of Fan and Ahmadi [2], the earlier simulation of Majlesara et al. [9], and the experimental data of Montogomery and Corn [32] and Kvansak et al. [33].

Particle deposition velocities in the horizontal wavy channel with $\lambda = 62.8$ mm for wave amplitudes of $a = 1$, 2, and 3 mm are evaluated. For the wavy channel, again, 5000 particles (the same number as that for the flat channel) were injected across the duct near the wall. In the channel with $\frac{2a}{\lambda} = 0.0318$ ($a = 1$ mm), the flow was rather smooth and particles were injected within the distance of $y^+ = 30$ ($y = 0.00163$ m) from the wall, whereas in the other two channels with wave amplitudes of $a = 2$ and 3 mm, particles were released within the distance of $y^+ = 45$ from the wall. The

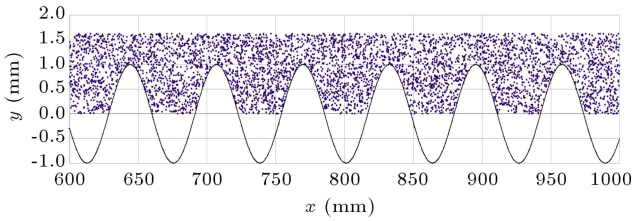

Figure 14. Distribution of particles in wavy wall channel with $\frac{2a}{\lambda} = 0.0318$ ($a = 1$ mm).

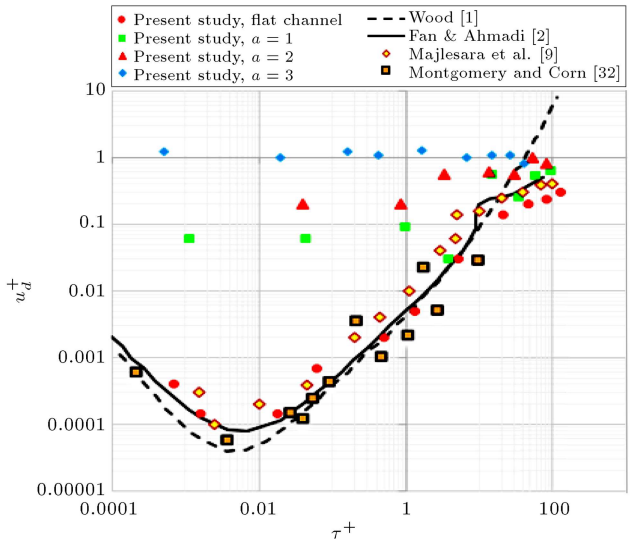

Figure 15. Non-dimensional particle deposition rate on wavy walls with different values of wave amplitude for the wavelength of $\lambda = 62.8$ mm.

initial distribution of particles in the wavy wall channel with $\frac{2a}{\lambda} = 0.0318$ ($a = 1$ mm) is shown in Figure 14.

Since wall shear stress and shear velocity varied on the surface of wavy channel, the effective shear velocity based on average wall shear stress along the entire channel was used in the present study. For different wavy wall channels, the deposition rates of particles predicted by the present v2f model are shown in Figure 15 and compared with the earlier experimental data and the predictions of empirical equations. It is seen that for large particles with $\tau^+ > 10$, the dimensionless deposition velocity is somewhat higher than that for the flat channel. This is because in this size range, inertia and gravity markedly affect the deposition velocity, and the majority of particles are deposited irrespective of the nature of the wall waviness. For particles with $0.1 < \tau^+ < 10$, however, the effect of wall waviness is very important. As the amplitude of the wall waviness increases, the particle deposition sharply increases compared to the flat wall due to impaction process. For $\tau^+ < 1$, the curvature of the windward face of the channel wall causes the particles to get close to the wall and the interception and diffusion mechanisms lead to particle deposition. Figure 15 also shows that the rate of particle deposition

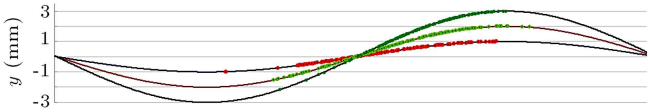

Figure 16. Locations of deposition of particles on the wavy wall of the channel.

generally increases as the wave amplitude increases for a fixed wavelength of the channel wall.

Deposition locations of 50 μm particles, which have a density ratio of $S = 2000$, on one wave cycle with different amplitudes are shown in Figure 16. It is seen that most of these relatively large particles are deposited on the windward region of the wave due to the impaction process. This region also has positive values of wall shear stress.

Figure 17 shows the number of deposited particles at times t and t^+. In reporting the number of deposited particles at t, it is observed that the slope of the curve generally increases as the wave amplitude increases for a fixed wavelength or wavelength decreases for a fixed amplitude. That is, increasing the roughness increases the deposition rate (there is an exception for $a = 2$ mm and $a = 3$ mm due to the formation of recirculation regions). However, in presenting the number of deposited particles at the dimensionless time t^+, the slope of the curve decreases as amplitude increases for a fixed wavelength, which is because of the sharp increase in the average value of the wall shear (for $a = 3$ mm and $\lambda = 20$ mm, $\tau_w = 0.6$ Pa; and for $a = 3$ mm and $\lambda = 62.8$ mm, $\tau_w = 0.04$ Pa; also, $t^+ = tu^{*^2}/\nu$). For a fixed length scale, however, Figure 17 shows that N_d increases as the wave amplitude increases.

To understand the effect of variation of wavelength on particle deposition, the deposition rates of particles for different channels with fixed wave amplitude of 3 mm and different wavelengths are investigated, and the results are shown in Figure 18 and compared with earlier results. It is seen that by decreasing the wavelength, the particle deposition velocity, u_d^+, decreases. As noted before in the discussion of Figure 17, the decrease is because of the high value of the mean wall shear stress, τ_w; but, in fact, the total deposition rate increases by decreasing the wavelength. Figures 15 and 18 for the variations of deposition velocity show that the rate of particle deposition increases as the ratio of $\frac{2a}{\lambda}$ increases. This is consistent with the known fact that the deposition on rough wall channels is higher than that in smooth channel [2]. That is, the wall waves act as surface roughness.

5. Conclusions

In this study, the turbulent flow conditions and particle deposition in a wavy channel flow were studied. Par-

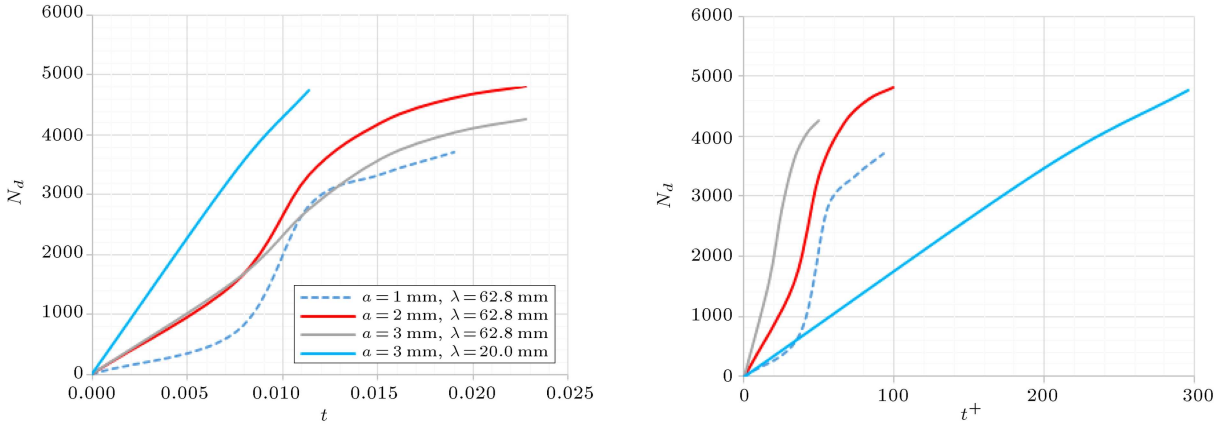

Figure 17. Number of deposited particles versus time.

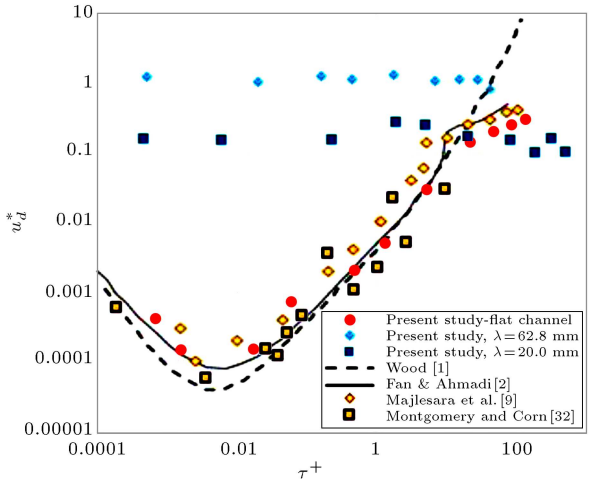

Figure 18. Effects of variation of wall wavelength, λ, on particle deposition velocity (wave amplitude of $a = 3$ mm).

ticular attention was devoted to the influence of the wavy wall on deposition rate of particles. Different wall wavelengths and wave amplitudes were considered. To simulate the turbulent flow field through the wavy channels, v2f turbulence model was used. The Kraichnan Gaussian Random Field model was used for simulating the instantaneous velocity fluctuations.

The main conclusions of the study are:

- The v2f turbulent model is capable of predicting the anisotropic features of turbulent flow in wavy channels;
- In order to obtain sufficiently accurate flow profiles, it is necessary to use very fine mesh near wavy walls with y^+ of about 0.2;
- Wavy walls cause significant variation of the wall shear stress, which could become negative due to the formation of recirculation regions;
- The deposition rate of particles with $\tau^+ < 10$ significantly increases with increase in the wall wave amplitude for fixed wavelength;
- Non-dimensional deposition velocity of particles with $\tau^+ > 10$ moderately increases with increase in $2a/\lambda$ due to the dominance of inertia and gravity effects;
- For fixed wave amplitude, decreasing the wavelength increases the deposition rate;
- Changing the wall wave amplitude markedly affects the deposition rate when the wavelength is constant;
- As the particles become larger, the dependency of their trajectory on the geometry diminishes.

Acknowledgements

This article is dedicated to Professor Abolhassan Vafai for establishing Scientia Iranica and for his life-long contributions to the expansion of international collaborations on engineering education and research.

References

1. Wood, N.B. "A simple method for the calculation of turbulent deposition to smooth and rough surfaces", *Aerosol Sci.*, **12**, pp. 275-290 (1981).
2. Fan, F.G. and Ahmadi, G. "A sublayer model for turbulent deposition of particles in vertical ducts with smooth and rough surfaces", *Aerosol Sci.*, **24**, pp. 45-64 (1992).
3. Li, A. and Ahmadi, G. "Computer simulation of deposition of aerosols in a turbulent channel flow with rough walls", *Aerosol Science and Technology*, **18**(1), pp. 11-24 (1993).
4. Tian, L. and Ahmadi, G. "Particle deposition in turbulent duct flows - comparison of different model prediction", *Aerosol Science*, **38**, pp. 377-397 (2007).
5. Zhang, Z. and Chen, Q. "Prediction of particle deposition onto indoor surfaces by CFD with a modified Lagrangian method", *Atmospheric Environment*, **43**, pp. 319-328 (2009).

6. Gao, R. and Li, A. "Modeling deposition of particles in vertical square ventilation duct flows", *Building and Environment*, **46**, pp. 245-252 (2010).

7. Sun, K., Lu, L., and Jiang, H. "A computational investigation of particle distribution and deposition in a 900 bend incorporating a particle-wall model", *Building and Environment*, **46**, pp. 1251-1262 (2010).

8. Gao, N., Niu, J., Zhu, T., and Wu, J. "Using RANS in turbulent models and Lagrangian approach to predict particle deposition in turbulent channel flows", *Building and Environment*, **48**, pp. 206-214 (2012).

9. Majlesara, M., Salmanzadeh, M., and Ahmadi, G. "A model for particles deposition in turbulent inclined channels", *Journal of Aerosol Science*, **64**, pp. 37-47 (2013).

10. Cherukat, P., Na, Y., and Hanratty, T.J. "Direct numerical simulation of a fully developed turbulent flow over a wavy wall", *Theoret. Comput. Fluid Dynamics*, **11**, pp. 109-134 (1998).

11. Yoon, H.S., El-Samni, O.A., Huynh, A.T., et al. "Effect of wave amplitude on turbulent flow in a wavy channel by direct numerical simulation", *Ocean Engineering*, **36**, pp. 697-707 (2009).

12. Errico, O. and Stalio, E. "Direct numerical simulation of turbulent forced convection in a wavy channel at low and order one Prandtl number", *International Journal of Thermal Sciences*, **86**, pp. 374-386 (2014).

13. Lu, H. and Lu, L. "Numerical investigation on particle deposition enhancement in duct air flow by ribbed wall", *Building and Environment*, **85**, pp. 61-72 (2014).

14. Lu, H. and Lu, L. "A numerical study of particle deposition in ribbed duct flow with different rib shapes", *Building and Environment*, **94**, pp. 43-53 (2015).

15. Ni, P., Jonsson, L.T.I., Ersson, M., and Jönsson, P.G. "Deposition of particles in liquid flows in horizontal straight channels", *International Journal of Heat and Fluid Flow*, **62**, pp. 166-173 (2016).

16. Wang, F., Zhang, E., and Wang, J. "A study of particle deposition in ventilation ducts with convex or con-cave wall cavity", *Procedia Engineering*, **205**, pp. 3285-3292 (2017).

17. Dritselis, C.D. "Numerical study of particle deposition in a turbulent channel flow with transverse roughness elements on one wall", *International Journal of Multiphase Flow*, **91**, pp. 1-18 (2017).

18. Dritselis, C.D. "On the enhancement of particle deposition in turbulent channel airflow by a ribbed wall", *Advanced Powder Technology*, **28**, pp. 922-931 (2017).

19. Li, Y., Gu, W., Wang, D., and He, J. "Direct numerical simulation of polydisperse aerosol particles deposition in low Reynolds number turbulent flow", *Annals of Nuclear Energy*, **12**(1), pp. 223-231 (2018).

20. Ho, P.Y., Cheng, C.K., and Huang, K.H. "Combined effects of thermophoresis and electrophoresis on particle deposition in mixed convection flow onto a vertical wavy plate", *International Communications in Heat and Mass Transfer*, **101**, pp. 116-121 (2019).

21. Gu, W., Wang, D., Li, Y., He, J., and He, Y. "A stochastic method in simulating particles transport and deposition in wall-bounded turbulent flow", *Annals of Nuclear Energy*, **127**, pp. 12-18 (2019).

22. Lu, H., Zhang, L.Z., Lu, L., and Pan, A. "Numerical investigation on monodispersed particle deposition in turbulent duct flow with thermophoresis", *Energy Procedia*, **158**, pp. 5711-5716 (2019).

23. Wang, Y., Yao, J., and Zhao, Y. "Large eddy simulation of particle deposition and resuspension in turbulent duct flows", *Advanced Powder Technology*, **30**(3), pp. 656-671 (2019).

24. Durbin, P.A. "Near-wall turbulent closure modeling without damping function", *Theoret. Comput. Fluid Dynamics*, **3**, pp. 1-13 (1991).

25. Kraichnan, R.H. "Diffusion by random velocity field", *Phys. Fluids*, **11**, pp. 22-31 (1970).

26. Davies, J.T., *Turbulence Phenomena*, Academic Press, New York (1972).

27. Saffman, P.G. "The lift on a small sphere in a slow shear flow", *J. fluid Mech.*, **22**, pp. 385-400 (1965).

28. Philips, D.A., Rossi, R., and Iaccarino, G. "The influence of normal stress anisotropy in predicting scalar dispersion with the v2-f model", *International Journal of Heat and Fluid Flow*, **32**, pp. 943-963 (2011).

29. Moser, R.D., Kim, J., and Mansour, N.N. "Direct numerical simulation of turbulent channel flow up to $Re\tau = 590$", *Phys. Fluids*, **11**, pp. 943-945 (1999).

30. Ounis, H., Ahmadi, G., and Mclaughlin, J.B. "Brownian particle deposition in a directly simulated turbulent channel flow", *Physics of Fluids A*, **5**, pp. 1427-1432 (1993).

31. Hudson, J.D. "The effect of a wavy boundary on turbulent flow", Ph.D. Thesis, University of Illinois, Urbana, IL, USA (1993).

32. Montogomery, T.L. and Corn, M. "Aerosol particle deposition in a pipe with turbulent flows", *Chemical Engineering Research and Design*, **62**, pp. 185-194 (1970).

33. Kvansak, W., Ahmadi, G., Bayer, R., and Gaynes, M. "Experimental investigation of duct particle deposition in a turbulent channel flow", *Journal of Aerosol Science*, **24**, pp. 795-815 (1993).

Biographies

Hamideh Hayati received her MSc degree in Chemical Engineering from Shahid Bahonar University, Kerman, Iran, and is now PhD candidate in Chemical Engineering at Oklahoma State University, Stillwater, Oklahoma, USA. Her research work concerns particle

deposition and dispersion in human airway.

Ataallah Soltani Goharrizi received his PhD from Shiraz University, Shiraz, Iran, and is now a professor of Chemical Engineering at Shahid Bahonar University, Kerman, Iran. His research work concerns aerosol, particle tracing, biomechanics, and CFD.

Mazyar Salmanzadeh received his PhD degree in Mechanical Engineering from Shahid Bahonar University, Kerman, Iran, and is now an associate professor of Mechanical Engineering at Shahid Bahonar University, Iran. His research work concerns particle deposition and dispersion as well as turbulent flow.

Goodarz Ahmadi received his PhD degree in Mechanical Engineering from the Purdue University, West Lafayette, IN, USA, and is now a Distinguished Professor and Robert R. Hill Professor of Mechanical and Aeronautical Engineering at Clarkson University, USA. He is a fellow of ASME, ATFE, ISME, and ISCE. He was the recipient of the 2016 ASME Freeman Scholar Award. He was also elected for the Iranian Science and Culture Hall of Fame in Mechanical Engineering in 2003. His research interests include multiphase flows, particle transport and deposition, turbulence, flow control, granular flows, air pollution, flow through porous and fractured media, random vibrations, and structural mechanics. He has held many administrative positions at Clarkson University including MAE Department Chair during 1992-1995, Associate Dean of Engineering during 2003-2005, Interim Vice Provost for Research during 2004-2005, and Dean of Engineering during 2005-2015. Earlier, he served as Associate Dean and Dean of Engineering at Shiraz University.